Efficient Extension to Quadrilateral Element of Three Field Hu-Washizu 2D Elasticity Formulation Based on Biorthogonal Systems

M.Pingaro[1,*]

Abstract

New quadrilateral mixed finite element based on modified Hu-Washizu formulation are presented. Hu-Washizu is a three field formulation where the unknowns are: displacement, stress and strain. The stability and consistency of the element are obtained by adding different types of bubble functions at the displacement field. Different types of bubble functions are successfully investigated and analyzed. In order to obtain an efficient discretization scheme, we use a pair of finite element bases forming a biorthogonal system between strain and stress. The biorthogonality relation allows us to statically condense out the strain and stress from the saddle-point system leading to a symmetric and positive-definite system. The strain and stress can be recovered in a post-processing step simply by inverting a diagonal matrix. Numerical examples prove the efficiency and the stability of the elements in the case of incompressible limit and distorted meshes.

Keywords: mixed finite elements, quadrilateral element, Hu-Washizu, biorthogonal systems, elasticity.

1. Introduction

In the linear and non-linear elasticity when the Lamé constant λ tends to infinity the standard finite element exhibit some problems of convergence as locking phenomena. In this context mixed formulations are used effectively to solve this inconvenient. One of the most popular mixed formulation

*Corresponding author.
Email address: marco.pingaro@iusspavia.it (M.Pingaro)
[1]Department of Civil Engineering and Architecture, University of Pavia, Pavia, Italy

adopted is the Hellinger-Reissner formulation, which one describe the problem adopting as variables the stresses and the displacements. This type of formulation requires the fulfillment of the inf-sup condition as described in D.Boffi et al. (2013). Employing the Hellinger-Reissner formulation many elements have been created such as D.N.Arnold and R.Winther (2002) for triangle elements and D.N.Arnold and G.Awanou (2005) for quadrilateral. Another type of mixed formulation is the Hu-Washizu formulation (see H.Hu (1955); K.Washizu (1982)) that it is a three-field formulation introduced by B.M.Fraeijs de Veubeke (1951). One examples of Hu-Washizu formulation applied at linear and non-linear elasticity using quadrilaterals and hexahedra are reported in E.P. Kasper and R.L. Taylor (2000). In B.P.Lamichhane et al. (2006) are showed that the modify Hu-Washizu formulation are able to obtaining uniform convergence of the finite element approximation in the nearly incompressible regime in the case of quadrilateral elements. The goal of this work is to present an extension of the modified three-field formulation Hu-Washizu presented in B.P.Lamichhane (2009) using the quadrilateral elements. In accordance to B.P.Lamichhane et al. (2013) we adopt the idea to create a biorthogonal system between the stresses and strains. This assumption is essentially for the static condensation of the stresses and strains for obtain a linear system in the only unknown displacement field. In order to ensure the stability of the element we enrich the space of displacement field with different type of bubble functions in accordance to W.Bai (1997); B.P.Lamichhane (2015) for the Stokes problem. In W.Bai (1997) we adopt two bubble functions to stabilize the element, while in B.P.Lamichhane (2015) use one single bubble function are adopted.

The structure of the paper is the following: first of all in Section 2 we recall the basic equations of linear elastic problem, Section 3 we briefly recall the modified Hu-Washizu formulations as in B.P.Lamichhane et al. (2013), Section 4 we develop the novel finite element spaces adopted. Finally, Section 5 we report many examples to prove the efficiency of the studied element and Section 6 the final remarks and the future developments.

2. Linear elastic continuum problem

In this section we briefly recovery the equations governing the homogeneous isotropic linear elastic material body.

Let a bounded domain $\Omega \in \mathbb{R}^n$ with Lipschitz boundary $\Gamma = \Gamma_d \cup \Gamma_n$, where Γ_d and Γ_n are the Dirichlet and Neumann boundaries, respectively.

The equilibrium equation is:

$$-\mathrm{div}(\boldsymbol{\sigma}) = \boldsymbol{f} \ , \tag{1}$$

where $\boldsymbol{\sigma}$ is the Cauchy stress tensor and $\boldsymbol{f}$ is the body forces per unit area or volume. The small strain tensor $\boldsymbol{d}$ is defined by:

$$\boldsymbol{d} = \boldsymbol{\varepsilon}(\boldsymbol{u}) = \frac{1}{2}(\boldsymbol{\nabla}\ \boldsymbol{u} + \boldsymbol{\nabla}\ \boldsymbol{u}^T) \ , \tag{2}$$

where $\boldsymbol{u}$ is the displacement field and $\boldsymbol{\nabla}$ is the gradient operator. In the case of linear elasticity we have:

$$\boldsymbol{\sigma} = \lambda\, \mathrm{tr}(\boldsymbol{\varepsilon})\boldsymbol{I} + 2\mu\, \boldsymbol{\varepsilon} \ , \tag{3}$$

where μ and λ are the Lamé parameters depending by the material, $\mathrm{tr}(\boldsymbol{a})$ is the trace of the tensor $\boldsymbol{a}$ and $\boldsymbol{I}$ is the identity tensor. Using the equation (3) and by some algebra one obtains:

$$\boldsymbol{\sigma} = \begin{pmatrix} \lambda(\varepsilon_{11} + \varepsilon_{22}) & 0 \\ 0 & \lambda(\varepsilon_{11} + \varepsilon_{22}) \end{pmatrix} + 2\mu \begin{pmatrix} \varepsilon_{11} & \varepsilon_{12} \\ \varepsilon_{12} & \varepsilon_{22} \end{pmatrix} , \tag{4}$$

and rearranging the equation (4):

$$\boldsymbol{\sigma} = \begin{pmatrix} (\lambda + 2\mu)\varepsilon_{11} + \lambda\, \varepsilon_{22} & 2\mu\, \varepsilon_{12} \\ 2\mu\, \varepsilon_{12} & (\lambda + 2\mu)\, \varepsilon_{22} + \lambda\, \varepsilon_{11} \end{pmatrix} . \tag{5}$$

Using the equations (1), (2) and (3) we obtain the resuming system for the linear elastic problem:

$$\begin{cases} \mathrm{div}(\boldsymbol{\sigma}) + \boldsymbol{f} = \boldsymbol{0} \ , \\ \boldsymbol{\varepsilon}(\boldsymbol{u}) - \boldsymbol{d} = \boldsymbol{0} \ , \\ \boldsymbol{\sigma} - \mathbf{C}\boldsymbol{d} = \boldsymbol{0} \ , \end{cases} \tag{6}$$

where $\mathbf{C}$ is the fourth order elastic tensor. On the boundary we have:

$$\begin{aligned} \boldsymbol{u}_d &= \overline{\boldsymbol{u}} \ , & \forall \boldsymbol{u} \subset \Gamma_d \ , \\ \boldsymbol{u}_n &= \boldsymbol{t} \cdot \boldsymbol{n} \ , & \forall \boldsymbol{u} \subset \Gamma_n \ , \end{aligned} \tag{7}$$

where $\boldsymbol{t}$ are the distributed traction and $\boldsymbol{n}$ is the unit normal vector along the Neumann boundary and $\overline{\boldsymbol{u}}$ is the prescribed displacement field along the Dirichlet boundary.

3. Briefly introduction to modify Hu-Washizu

Starting by the equations resumed in the system (6), need be tested with triplet of virtual displacements, strains, stresses, say $(\boldsymbol{v}, \boldsymbol{e}, \boldsymbol{\tau})$ to arrive at the classical Hu-Washizu variational principle reads:

$$\begin{cases} -\int_\Omega \sigma : \boldsymbol{\varepsilon}(\boldsymbol{v}) + \int_\Omega \boldsymbol{f} \cdot \boldsymbol{v} = 0\,, & \forall \boldsymbol{v} \in V \\ \int_\Omega (\boldsymbol{\varepsilon}(\boldsymbol{u}) - \boldsymbol{d}) : \boldsymbol{\tau} = 0\,, & \forall \boldsymbol{\tau} \in S_0 \\ \int_\Omega \boldsymbol{\sigma} : \boldsymbol{e} - \int_\Omega \mathbf{C}\boldsymbol{d} : \boldsymbol{e} = 0\,, & \forall \boldsymbol{e} \in S \end{cases} \tag{8}$$

where we define the spaces $V = [H_0^1(\Omega)]^n$, $S = L^2(\Omega)^{n\times n}_{sym}$ and

$$S_0 = \left\{ \boldsymbol{\tau} \in S \;\mid\; \int_\Omega \boldsymbol{\tau} : \boldsymbol{I} = 0 \right\}\,. \tag{9}$$

The Hu-Washizu problem reads: Find $(\boldsymbol{u}, \boldsymbol{d}, \boldsymbol{\sigma}) \in V \times S \times S_0$ such that:

$$\begin{cases} \tilde{a}((\boldsymbol{u}, \boldsymbol{d}), (\boldsymbol{v}, \boldsymbol{e})) + b((\boldsymbol{v}, \boldsymbol{e}), \boldsymbol{\sigma}) = l(\boldsymbol{v})\,, & \forall\,(\boldsymbol{u}, \boldsymbol{d}) \in V \times S \\ b((\boldsymbol{u}, \boldsymbol{d}), \boldsymbol{\tau}) = 0\,, & \forall \boldsymbol{\tau} \in S_0 \end{cases} \tag{10}$$

Due to the lack of ellipticity of the bilinear form $\tilde{a}((\boldsymbol{u}, \boldsymbol{d}), (\boldsymbol{v}, \boldsymbol{e}))$ on the space $V \times S$, as you can see in B.P.Lamichhane et al. (2013) and B.P.Lamichhane (2009), a positive scalar α is introduced so as the replace the bilinear form from $\tilde{a}((\boldsymbol{u}, \boldsymbol{d}), (\boldsymbol{v}, \boldsymbol{e}))$ with

$$a((\boldsymbol{u}, \boldsymbol{d}), (\boldsymbol{v}, \boldsymbol{e})) = \int_\Omega \boldsymbol{d} : \boldsymbol{C}\boldsymbol{e} + \alpha \int_\Omega (\boldsymbol{\varepsilon}(\boldsymbol{u}) - \boldsymbol{d}) : (\boldsymbol{\varepsilon}(\boldsymbol{v}) - \boldsymbol{e})\,. \tag{11}$$

By so doing, one ends up with the following stable Hu-Washizu continuous formulation: Find $(\boldsymbol{u}, \boldsymbol{d}, \boldsymbol{\sigma}) \in V \times S \times S_0$ such that:

$$\begin{cases} a((\boldsymbol{u}, \boldsymbol{d}), (\boldsymbol{v}, \boldsymbol{e})) + b((\boldsymbol{v}, \boldsymbol{e}), \boldsymbol{\sigma}) = l(\boldsymbol{v})\,, & \forall\,(\boldsymbol{u}, \boldsymbol{d}) \in V \times S \\ b((\boldsymbol{u}, \boldsymbol{d}), \boldsymbol{\tau}) = 0\,, & \forall \boldsymbol{\tau} \in S_0 \end{cases} \tag{12}$$

4. Finite element discretization

We consider a quasi-uniform triangulation $\mathcal{T}_h$ of the polygonal domain Ω consists of simply, either quadrilateral or hexahedral. We take into account of standard bilinear finite element space $K_h \subset H^1(\Omega)$ defined on the triangulation $\mathcal{T}_h$, where:

$$K_h := \left\{ v \in C^0(\Omega) : v_{|T} \in \mathcal{Q}_1(T),\ T \in \mathcal{T}_h \right\}, \quad K_h^0 = K_h \cap H_0^1(\Omega), \tag{13}$$

and the space of bubble functions

$$B_h := \left\{ b_T \in H^1(T) : b_{T|\partial T} = 0 \text{ and } \int_T b_T \, dx > 0,\ T \in \mathcal{T}_h \right\}, \tag{14}$$

and we define the spaces for strain and displacement as $\boldsymbol{S}_h := [K_h]^{2\times 2}$ and $\boldsymbol{V}_h := [K_h^0 \bigoplus B_h]^2$. In the next section we discuss the different choosing of bubble functions. For the discrete stress space we use:

$$\boldsymbol{M}_h := \left\{ \boldsymbol{\tau}_h \in [M_h]^{2\times 2} : \int_\Omega \boldsymbol{\tau}_h : \mathbf{1} \, dx = 0 \right\} \subset \boldsymbol{S}_0 , \tag{15}$$

and let $\{\phi_1, \cdots, \phi_n\}$ and $\{\mu_1, \cdots, \mu_n\}$ the n the basis functions for the space V_h and M_h respectively, we construct the functions μ_i using the following biorthogonality property between the space V_h and M_h:

$$\int_\Omega \mu_i \phi_j \, dx = c_j \delta_{ij} , \ \ c_j \neq 0 , \ \ 1 \leq i, j \leq n , \tag{16}$$

where δ_{ij} is Kronecker symbol, and c_j is a scaling factor which can be chosen to be proportion al to the area of support of ϕ_j. The local basis function of K_h and M_h for the reference square element (see figure 1) $\hat{T} := \{(\xi, \eta) : -1 \leq \xi \leq 1 , -1 \leq \eta \leq 1\}$ are:

$$\begin{aligned} \hat{\phi}_1 &= \frac{1}{4}(1-\xi)(1-\eta) , \quad \hat{\phi}_2 = \frac{1}{4}(1+\xi)(1-\eta) , \\ \hat{\phi}_3 &= \frac{1}{4}(1+\xi)(1+\eta) , \quad \hat{\phi}_4 = \frac{1}{4}(1-\xi)(1+\eta) . \end{aligned} \tag{17}$$

and

$$\begin{aligned} \hat{\mu}_1 &= 1 - 3\xi - 3\eta + 9\xi\eta , \quad \hat{\mu}_2 = 1 + 3\xi - 3\eta - 9\xi\eta , \\ \hat{\mu}_3 &= 1 + 3\xi + 3\eta + 9\xi\eta , \quad \hat{\mu}_4 = 1 - 3\xi + 3\eta + 9\xi\eta . \end{aligned} \tag{18}$$

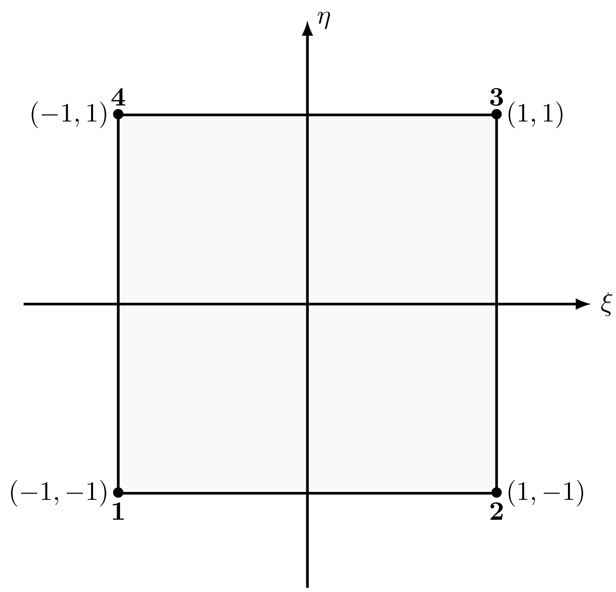

Figure 1: Reference Element

It is important to observe that the global basis functions of the space M_h are not continuous.

Now it is possible to write the weak discrete problem as: Find $(\boldsymbol{u}_h, \boldsymbol{d}_h, \boldsymbol{\sigma}_h) \in V_h \times S_h \times M_h$ such that:

$$\begin{cases} a((\boldsymbol{u}_h, \boldsymbol{d}_h), (\boldsymbol{v}_h, \boldsymbol{e}_h)) + b((\boldsymbol{v}_h, \boldsymbol{e}_h), \boldsymbol{\sigma}_h) = l(\boldsymbol{v}_h)\ , & \forall\, (\boldsymbol{u}_h, \boldsymbol{d}_h) \in V_h \times S_h \\ b((\boldsymbol{u},_h \boldsymbol{d}_h), \boldsymbol{\tau}_h) = 0\ , & \forall \boldsymbol{\tau}_h \in M_h \end{cases} \tag{19}$$

The matrix-vector form of the weak variational system (19) may then be written as

$$\begin{bmatrix} \alpha \boldsymbol{A} & -\alpha \boldsymbol{B} & \boldsymbol{W} \\ -\alpha \boldsymbol{B}^T & \boldsymbol{K} + \alpha \boldsymbol{M} & -\boldsymbol{D} \\ \boldsymbol{W}^T & -\boldsymbol{D}^T & \boldsymbol{0} \end{bmatrix} \begin{bmatrix} \boldsymbol{x}_u \\ \boldsymbol{x}_d \\ \boldsymbol{x}_\sigma \end{bmatrix} = \begin{bmatrix} \boldsymbol{b}_f \\ \boldsymbol{0} \\ \boldsymbol{0} \end{bmatrix}\ , \tag{20}$$

where

$$
\begin{aligned}
\boldsymbol{A} &= \int_\Omega \boldsymbol{\varepsilon}(\boldsymbol{u}_h) : \boldsymbol{\varepsilon}(\boldsymbol{v}_h)\,, & \boldsymbol{B} &= \int_\Omega \boldsymbol{d}_h : \boldsymbol{\varepsilon}(\boldsymbol{v}_h)\,, \\
\boldsymbol{W} &= \int_\Omega \boldsymbol{\sigma}_h : \boldsymbol{\varepsilon}(\boldsymbol{v}_h)\,, & \boldsymbol{K} &= \int_\Omega \boldsymbol{C}\boldsymbol{e}_h : \boldsymbol{d}_h\,, \\
\boldsymbol{M} &= \int_\Omega \boldsymbol{e}_h : \boldsymbol{d}_h\,, & \boldsymbol{D} &= \int_\Omega \boldsymbol{\sigma}_h : \boldsymbol{e}_h\,.
\end{aligned}
\tag{21}
$$

$\boldsymbol{D}$ is a diagonal matrix. Using the property in equation (16) it is possible to condense statically $\boldsymbol{x}_d$ and $\boldsymbol{x}_\sigma$, and we obtain the following system in only displacement unknown $\boldsymbol{x}_u$:

$$
\left[\alpha \boldsymbol{A} - \alpha\left(\boldsymbol{B}\boldsymbol{D}^{-1}\boldsymbol{W}^{-T} + \boldsymbol{W}\boldsymbol{D}^{-1}\boldsymbol{B}^T\right) + \boldsymbol{W}\boldsymbol{D}^{-1}\left(\boldsymbol{K} + \alpha\boldsymbol{M}\right)\boldsymbol{D}^{-1}\boldsymbol{W}^T\right]\boldsymbol{x}_u = \boldsymbol{b}_f, \tag{22}
$$

whereas strains and stresses may be evaluated afterwords by back-substitution.

4.1. Bubble functions

In this section we detail the different choosing of the bubble functions. Addition of the bubble functions is essential to create a stable space. Accordingly to W.Bai (1997) and B.P.Lamichhane (2015), we obtain four types of elements with different bubble functions. In the first two cases we use a modification of the standard bubble function ,that is for the reference element:

$$
\hat{b}_T(\xi,\eta) = (1-\xi^2)(1-\eta^2)\,, \tag{23}
$$

while in the next two, we add to the standard bubble function another one.

4.1.1. One Bubble function (type 1)

As a first choice of bubble function we use:

$$
\hat{b}_{T,1}(\xi,\eta) = c_T \cdot \phi_T(\xi,\eta) \cdot \hat{b}_T(\xi,\eta)\,, \tag{24}
$$

where c_T is a coefficient in order to obtain $\hat{b}_{T,1}(\xi_g,\eta_g) = 1$ (where $\boldsymbol{g}$ is the centroid of the elements), ϕ_K is the standard bilinear basis function corresponding to the lower-left corner of the square T. In the case of reference square element we obtain:

$$
\hat{b}_{T,1}(\xi,\eta) = (1-\xi)(1-\eta)(1-\xi^2)(1-\eta^2)\,. \tag{25}
$$

4.1.2. One Bubble function (type 2)

The second choice of bubble function we take:

$$\hat{b}_{T,1}(\xi,\eta) = c_T \cdot (a + b\xi + c\eta) \cdot \hat{b}_T(\xi,\eta) \,, \tag{26}$$

where $a, b, c \in \mathbb{R}$ and $a, b, c \neq 0$. For simplicity we should take $a = b = c = 1$ and we obtain for the reference square:

$$\hat{b}_{T,1}(\xi,\eta) = (1 + \xi + \eta)(1 - \xi^2)(1 - \eta^2) \,. \tag{27}$$

4.1.3. Two Bubble functions

Using two bubble functions, where the first is the standard bubble function and the second bubble is a modification of the standard bubble. We define a new space of bubble functions as follow:

$$\hat{B}_h^+ = \left\{ \hat{\boldsymbol{v}} \in B_h \;\middle|\; \hat{\boldsymbol{v}} = [\boldsymbol{v}_0 + \boldsymbol{v}_{01}(a\xi + b\eta)]\, \hat{b}_T \,, \boldsymbol{v}_0, \boldsymbol{v}_{01} \in \mathbb{R}^2 \right\} \,, \tag{28}$$

where a and b are two arbitrary constants satisfying $a^2 + b^2 \neq 0$. For the sake of simplicity should take $a = b = 1$. The two bubble functions are:

$$\begin{aligned} \hat{b}_{T,1}(\xi,\eta) &= \hat{b}_T \,, \\ \hat{b}_{T,2}(\xi,\eta) &= (\xi + \eta)\, \hat{b}_T \,. \end{aligned} \tag{29}$$

4.1.4. Two Bubble functions, which one mixed

As a finally choice of bubbles we use a standard bubble function plus one mixed bubble function for the two components of displacement. We define the modify space of bubble functions:

$$\hat{B}_h^{++} = \left\{ \hat{\boldsymbol{v}} \in B_h \;\middle|\; \hat{\boldsymbol{v}} = \left[\boldsymbol{v}_0 + w_0 \boldsymbol{\nabla} \hat{\phi}_1\right] \hat{b}_T,\ \boldsymbol{v}_0 \in \mathbb{R}^2,\ w_0 \in \mathbb{R} \right\} \,, \tag{30}$$

where $\boldsymbol{\nabla}\hat{\phi}_1$ is the gradient of the first shape function $\hat{\phi}$. The two bubble functions are:

$$\begin{aligned} \hat{b}_{T,1}(\xi,\eta) &= \hat{b}_T \,, \\ \hat{\boldsymbol{b}}_{T,2}(\xi,\eta) &= \left[\hat{\phi}_{1,\xi},\ \hat{\phi}_{1,\eta}\right] \hat{b}_T \,, \end{aligned} \tag{31}$$

where $\hat{\phi}_{1,\xi}$ $\hat{\phi}_{1,\eta}$ are the derivatives of the first shape function $\hat{\phi}$ to ξ and η respectively. We can observe that $\hat{\boldsymbol{b}}_{T,2}$ is a vector.

5. Numerical examples

In this section we report some examples using the presented formulation to proven the good behaviour. All examples are studied in nearly incompressible limit.

5.1. Square problem

First example is a unit square domain with homogeneous Dirichlet boundary conditions. This benchmark problem is analyzed in S.C. Brenner (1993). The Lamé constant are fix to $\nu = 0.49995$ and $\mu = 1$. We impose the following body forces:

$$\begin{aligned} f_1 = \beta \big(&\pi^2 \left(4 \sin(\pi y)\left(-1 + 2\cos(2\pi x)\right) - \cos\left(\pi\left(x+y\right)\right)\right. \\ &\left.+ A \sin(\pi x) \sin(\pi y)\right)\big) \ , \\ f_2 = \beta \big(&\pi^2 \left(4 \sin(2\pi x)\left(1 - 2\cos(2\pi y)\right) - \cos\left(\pi\left(x+y\right)\right)\right. \\ &\left.+ A \sin(\pi x) \sin(\pi y)\right)\big) \ , \end{aligned} \tag{32}$$

where

$$A = \frac{2}{1+\lambda} \ \text{and} \ \beta = \frac{1}{25} \ . \tag{33}$$

By imposition of the previously body forces the exact solution is:

$$\begin{aligned} u_1 &= \beta \left(\sin(2\pi y)\left(-1 + \cos(2\pi x)\right) + B\right) \ , \\ u_2 &= \beta \left(\sin(2\pi x)\left(1 - \cos(2\pi y)\right) + B\right) \ , \end{aligned} \tag{34}$$

where

$$B = 0.5 A \sin(\pi x) \sin(\pi y) \ . \tag{35}$$

The problem is studied using two type of mesh: first of all using a square mesh and before using a trapezoidal mesh. The two types of mesh are shown in figures 2(a) and 2(b). Figures 3(a), 3(b), 4(a) and 4(b) shown the error in norm L^2 in the case of regular mesh for the different types of bubble functions and coefficients α. All types of element converge in a good way. In Figures 5(a), 5(b), 6(a) and 6(b) we report the previously results in the case of trapezoidal meshes. In this example do not see an appreciable difference between the different choices of the α coefficient and types of mesh.

In figures 7(a), 7(b), 8(a), 8(b), 9(a), 9(b), 10(a) and 10(b) we report the error in L^2 norm of the strain d_{xx} for the the different choice of bubble functions and coefficient α.

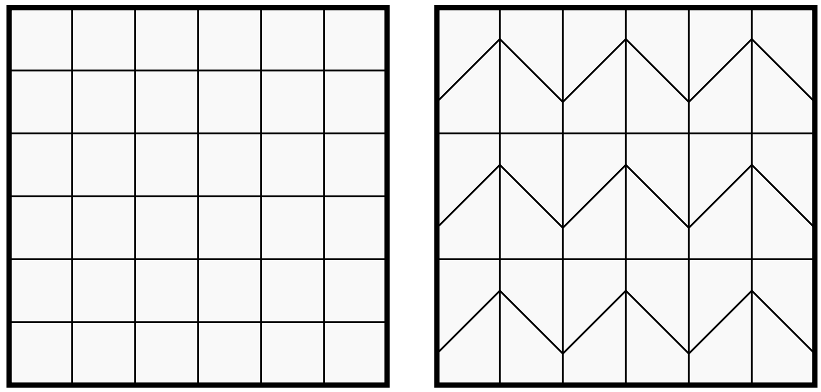

(a) Regular mesh (b) Trapezoidal mesh

Figure 2: Square Problem

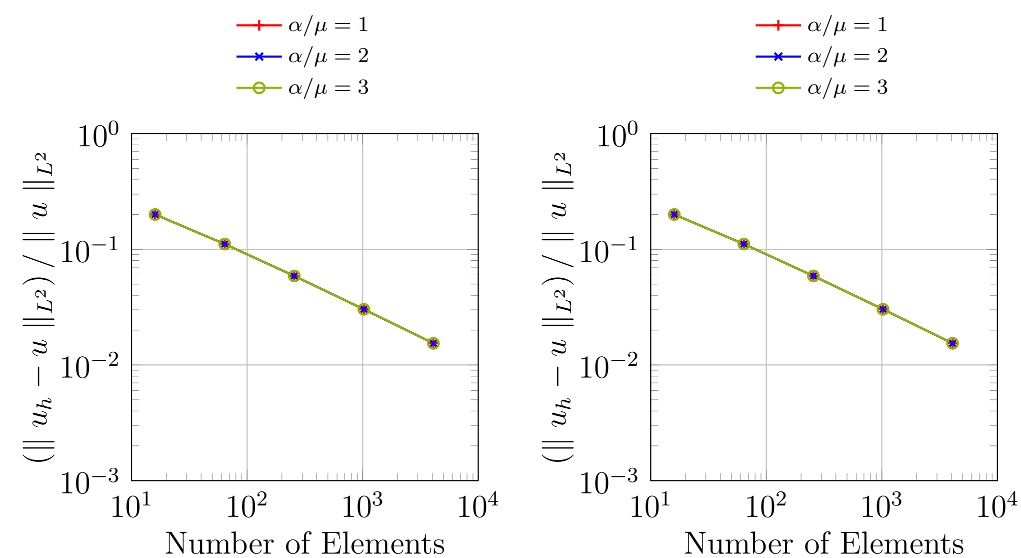

(a) type 1 (b) type 2

Figure 3: The relative error vs. the number of elements measured relative to the L^2 norm (Case one bubble function and regular mesh)

5.2. Cantilever beam problem

Now we consider the beam with length $L = 10$ and height $l = 2$ as we shown in figure 11. The Young modulus is set equal to $E = 1500$ and

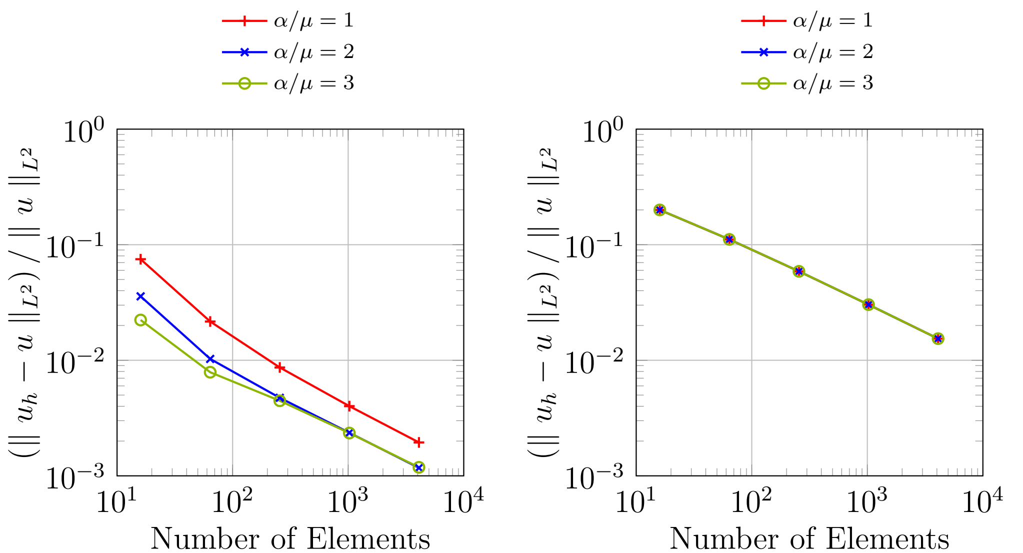

(a) Case two bubble function

(b) Case two bubble function of which one mixed

Figure 4: The relative error versus the number of elements measured relative to the L^2 norm (regular mesh)

the Poisson $\nu = 0.4999$. The beam are fixed in the bottom left corner and subjected to a distributed load with $f = 300$ on the right edge as shown in figure 11. The exact solution reported in J.K.Djoko and B.D.Reddy (2006) is:

$$
\begin{aligned}
u(x,y) &= \frac{2f}{El}(1-\nu^2)x\left(\frac{l}{2}-y\right) \; , \\
v(x,y) &= \frac{f}{El}\left[x^2+\frac{\nu}{1-\nu}\left(y^2-ly\right)\right] \; .
\end{aligned}
\tag{36}
$$

We use to model the beam two types of mesh: regular anf trapezoidal as in the previously example (see figures 2(a) and 2(b)).

In figure 12 is shown the deformation resulting using 2000 elements with two bubble functions while in figure 13 and 14 are shown the comparison between the computed strain component $[\boldsymbol{d}_h]_{xx}$ and $[\boldsymbol{d}_h]_{yy}$ and the analytic strain component $[\boldsymbol{d}]_{xx}$ and $[\boldsymbol{d}]_{yy}$. The computed strain components are in a good agreement with the analytical ones.

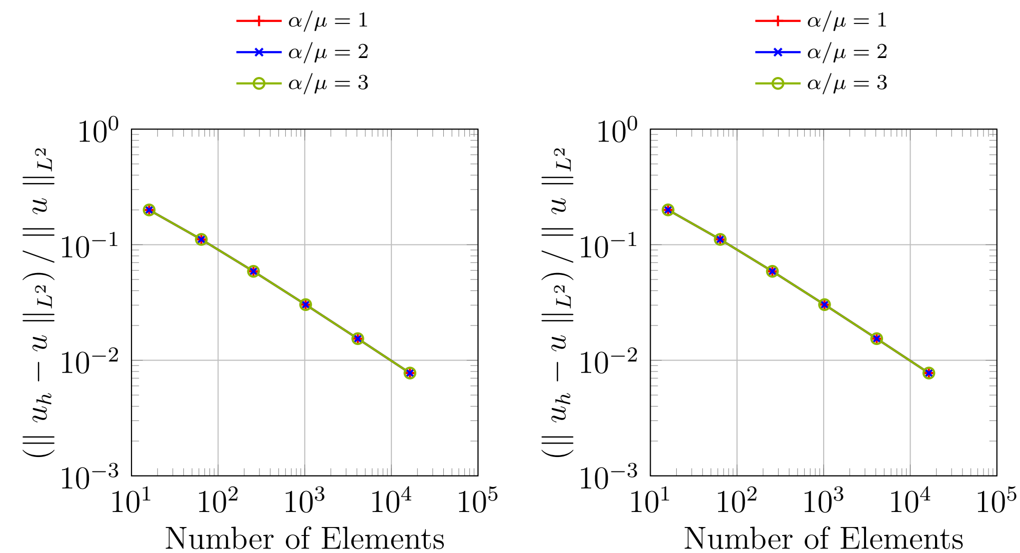

(a) type 1 (b) type 2

Figure 5: The relative error vs. the number of elements measured relative to the L^2 norm (Case one bubble function and Trapezoidal mesh)

In figures 17(a), 17(b), 18(a) and 18(b) are shown the L^2-norm error for different types of bubble functions used in the case of $\alpha/mu := 1, 2, 3$, while in figures 17(a), 17(b), 18(a) and 18(b) the same plots using trapezoidal meshes. In all examples the parameter α influences the magnitude of the relative error but not the rate of convergence. Furthermore the distorted elements have a negligible difference in comparison to the regular mesh.

5.3. Cook's membrane

The final example is the Cook's membrane. That is a typical benchmark and consist of a beam with vertex: $(0, 0)$, $(48, 44)$, $(48, 60)$ and $(0, 44)$. The left vertical edge is clamped and the right vertical edge subjected to the vertical distributed forces with resultant $F = 100$ as it shown in figure 19. The material properties are taken to be $E = 250$ and $\nu = 0.4999$, so that a nearly incompressible response is obtained. We report in figures 20(a), 20(b), 20(c) and 20(d) the vertical displacement of the point A versus the number of element per side for different choices of the parameter $\alpha = \{1, \mu, 2\mu, 3\mu\}$. The parameter α greatly influence the results, indeed, in the case of $\alpha = 1$,

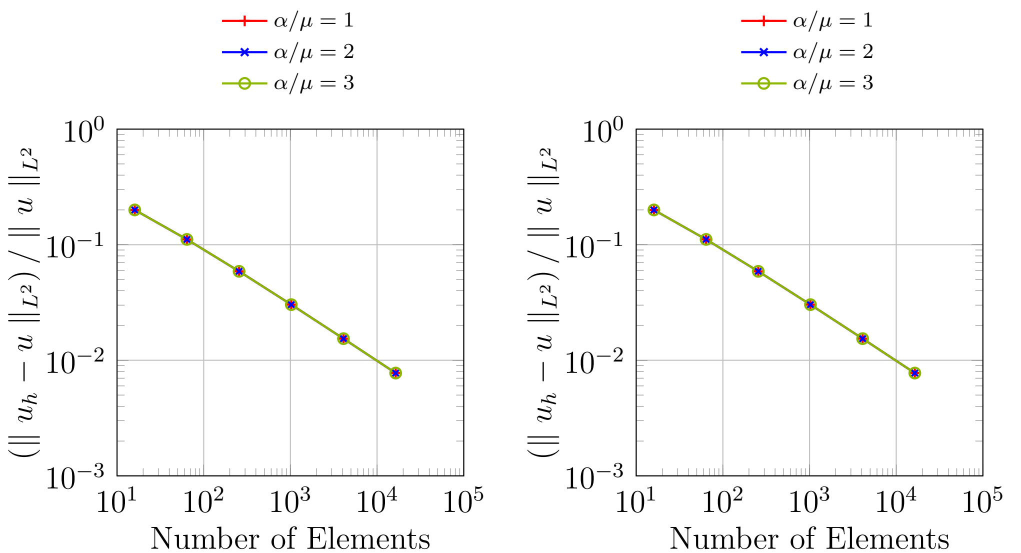

(a) Case two bubble function

(b) Case two bubble function of which one mixed

Figure 6: The relative error vs. the number of elements measured relative to the L^2 norm (Case one bubble function and Trapezoidal mesh)

figure 20(a), the obtained results are completely incorrect. However, the convergence is archived for all elements in the case of the normal range of the parameter α. No locking phenomenon is highlighted in any of the cases.

6. Conclusions

We present a new family of quadrilaterals mixed finite elements based on a modified Hu-Washizu formulation. Different types of enrichment of the displacement field were successfully tested in the case of incompressible regime and trapezoidal meshes.

The future developments are oriented to finding an optimal choosing of the parameter α and the extension to the 3-D case using hexahedral elements.

W.Bai. “The quadrilateral ‘Mini’ finite element for Stokes problem”, *Comput. Methods Appl. Mech. Engrg.*, 143: 41-47, 1997.

D.Boffi. “On the finite element method on quadrilateral meshes”, *Appl. Num. Mathematics*, 56: 1271-1282, 2006.

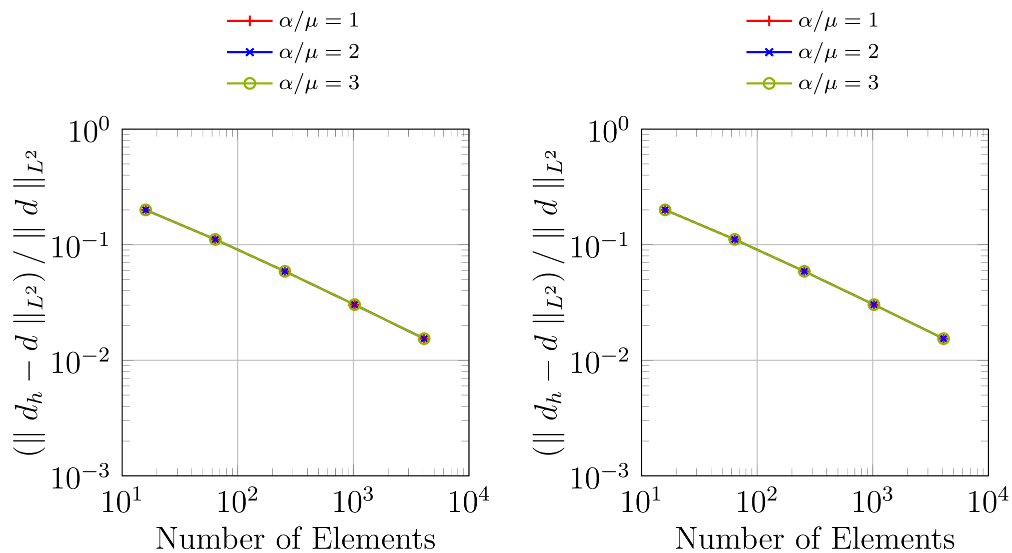

(a) Case regular mesh

(b) Case trapezoidal mesh

Figure 7: The relative error of strain $\boldsymbol{d}_{xx}$ vs. the number of elements (Case of two bubble functions)

B.P.Lamichhane. "A quadrilateral 'mini' finite element for the Stokes problem using a single bubble function", *Appl. Num. Math.*, 56: 1271-1282, 2015.

J.K.Djoko, B.D.Reddy. "An extended Hu-Washizu formulation for elasticity", *Comput. Methods Appl. Mech. Engrg.*, 195: 6330-6346, 2006.

B.P.Lamichhane, A.T.McBride, B.D.Reddy. "A finite element method for three-field formulation of linear elasticity based on biorthogonal systems", *Comput. Methods Appl. Mech. Engrg.*, 258: 109-117, 2013.

B.P.Lamichhane, B.D.Reddy, B.I.Wohlmuth. "Convergence in the incompressible limit of finite element approximation based on Hu-Washizu formulation", *Numer. Math.*, 104: 151-175, 2006.

D.Boffi, C.Lovadina. "Analisys of new augmented Lagrangian formulation for mixed finite element schemes", *Numer. Math.*, 75: 405-419, 1997.

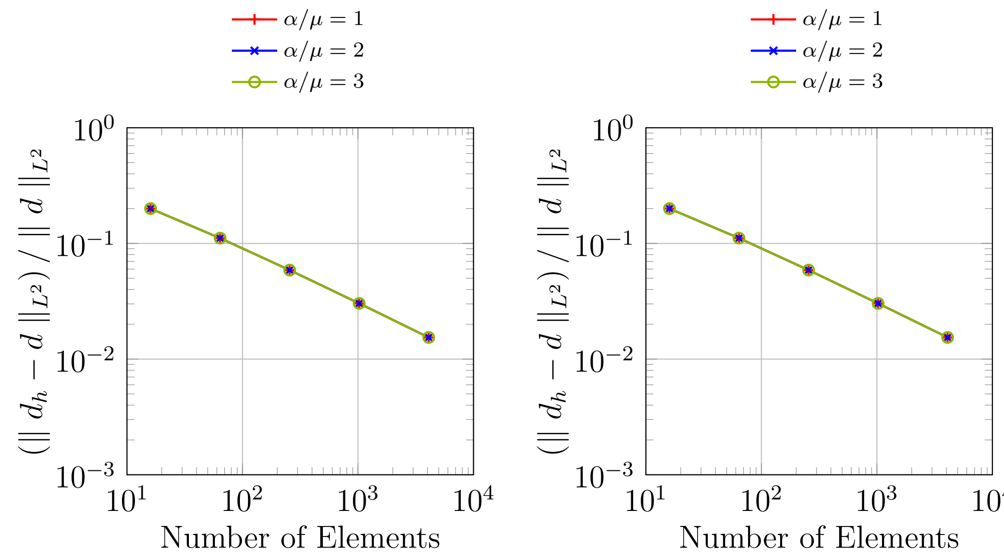

(a) Case regular mesh

(b) Case trapezoidal mesh

Figure 8: The relative error of strain $\boldsymbol{d}_{xx}$ vs. the number of elements (Case of two bubble functions, which one mixed)

B.P.Lamichhane. "From the Hu-Washizu formulation to the average nodal strain formulation", *Comput. Methods Appl. Mech. Engrg.*, 198: 3957-3961, 2009.

D.N.Arnold, R.Winther. "Mixed finite elements for elasticity", *Numer. Math.*, 92: 401-419, 2002.

D.Boffi, F.Brezzi, M.Fortin. "Mixed Finite Element Methods and Applications", *Springer Series in Computational Mathematics*, Vol.44, 2013.

D.N.Arnold, G.Awanou. "Rectangular mixed finite elements for elasticity", *Models Methods Appl. Sci.*, 15: 1417-1429, 2005.

H.Hu. "On some variational principles in the theory of elasticity and the theory of plasticity", *Sci. Sin.*, 4: 33-54, 1955.

K.Washizu. "Variational Methods in Elasticity and Plasticity, third ed.", *Pergamon Press*, 1982.

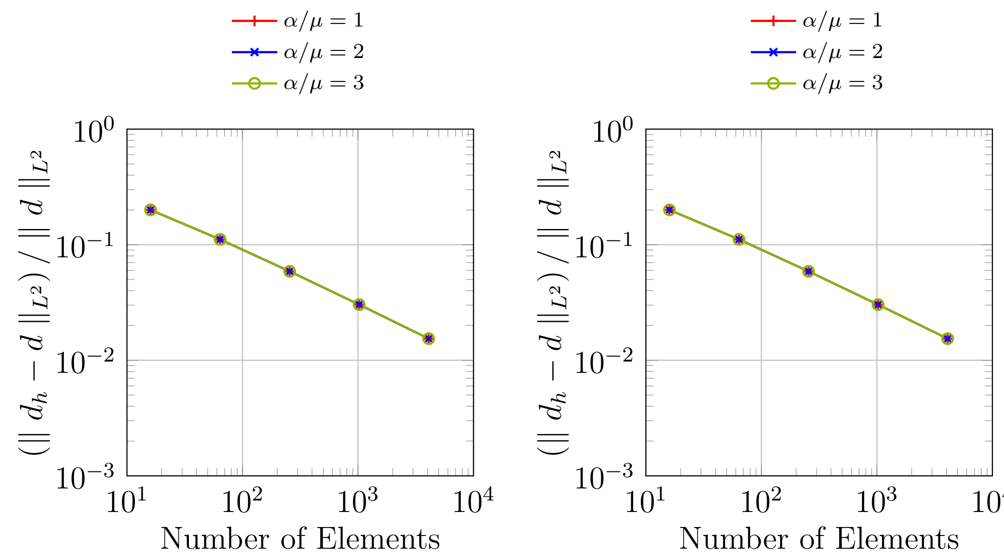

(a) Case regular mesh

(b) Case trapezoidal mesh

Figure 9: The relative error of strain $\boldsymbol{d}_{xx}$ vs. the number of elements (Case of one bubble function type 1)

B.M. Fraeijs de Veubeke. "Diffusion des inconnues hyperstatiques dans les voilures á longeron couplés", *Bull. Serv. Technique de l'Aeronautique Impremérie Marcel Hayez*, Bruxelles, 1951.

E.P. Kasper, R.L. Taylor. "A mixed-enhanced strain method Part I: geometrically linear problems", *Comput. Struct.*, 75: 237-250, 2000.

E.P. Kasper, R.L. Taylor. "A mixed-enhanced strain method Part II: geometrically nonlinear problems", *Comput. Struct.*, 75: 251-260, 2000.

S.C. Brenner. "A nonconforming mixed multigrid method for the pure displacement problem in planar linear elasticity", *SIAM J. Numer. Anal.*, 30: 116–135, 1993.

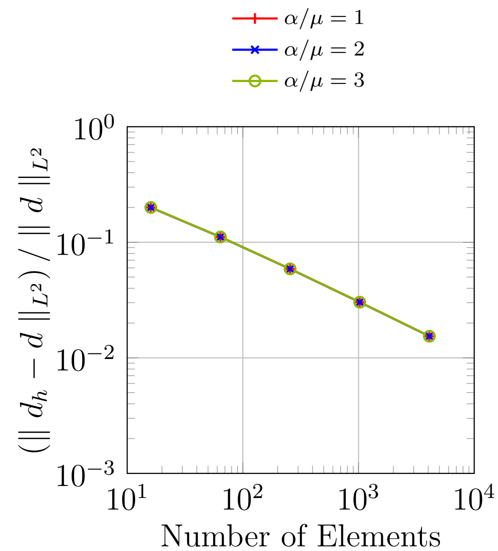

(a) Case regular mesh

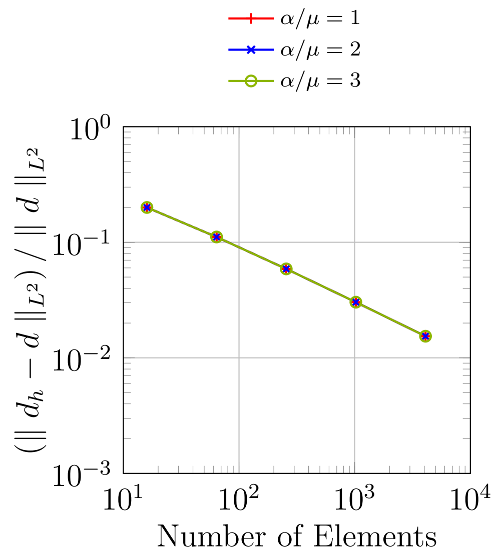

(b) Case trapezoidal mesh

Figure 10: The relative error of strain $\boldsymbol{d}_{xx}$ vs. the number of elements (Case of one bubble function type 2)

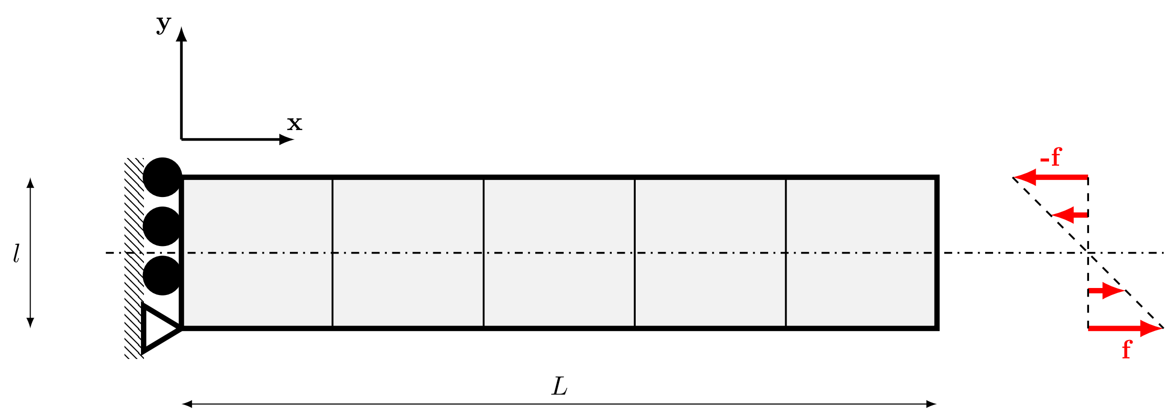

Figure 11: Beam cantilever geometry

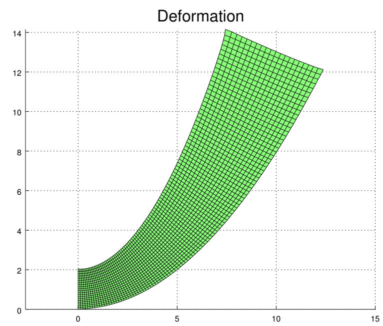

Figure 12: Beam Cantilever: deformation plot using 2000 elements with two bubble functions and $\alpha/\mu = 1$

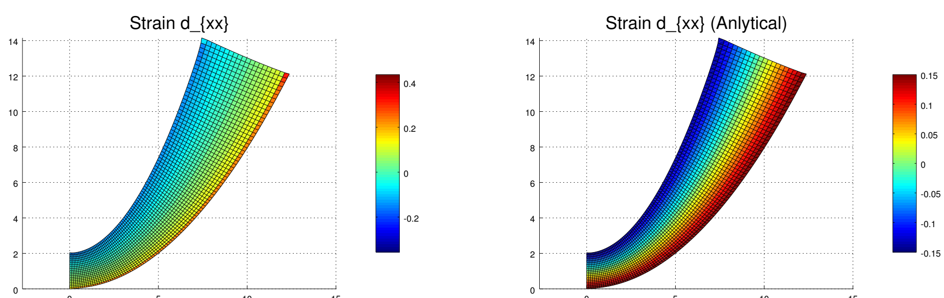

(a) Strain $\boldsymbol{d}_h$

(b) Strain $\boldsymbol{d}$

Figure 13: Beam Cantilever: strain $[\boldsymbol{d}_h]_{xx}$ vs. $[\boldsymbol{d}]_{xx}$ using 2000 elements with two bubble functions and $\alpha/\mu = 1$

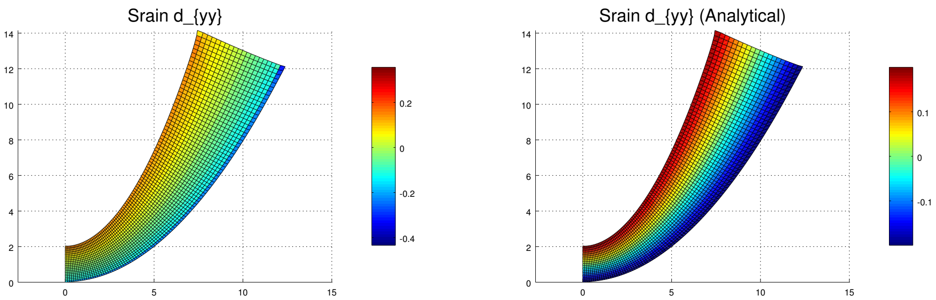

(a) Strain $\boldsymbol{d}_h$

(b) Strain $\boldsymbol{d}$

Figure 14: Beam Cantilever: strain $[\boldsymbol{d}_h]_{yy}$ vs. $[\boldsymbol{d}]_{yy}$ using 2000 elements with two bubble functions and $\alpha / = 1$

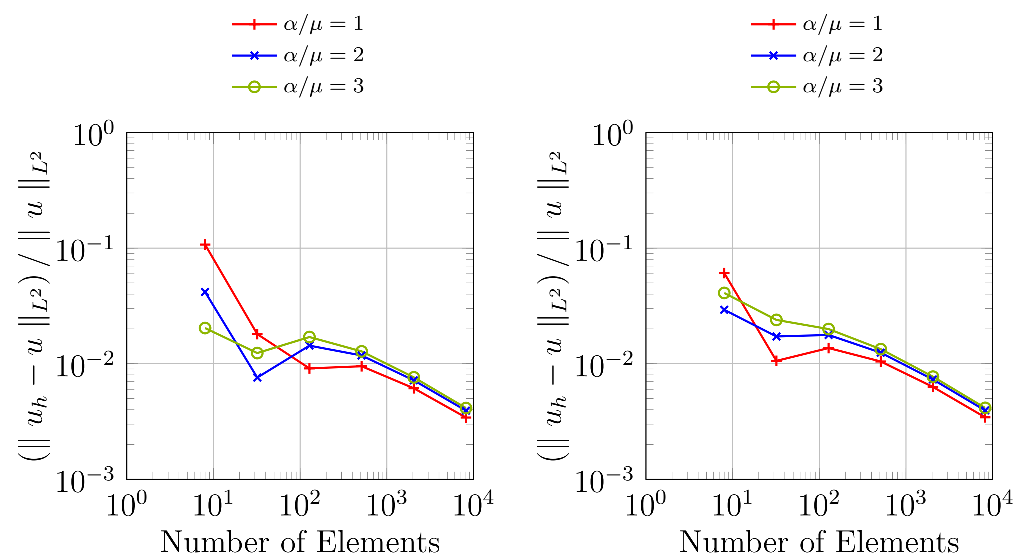

(a) Type 1

(b) Type 2

Figure 15: Beam Cantilever: the relative error vs. the number of elements measured relative to the L^2 norm (regular mesh)

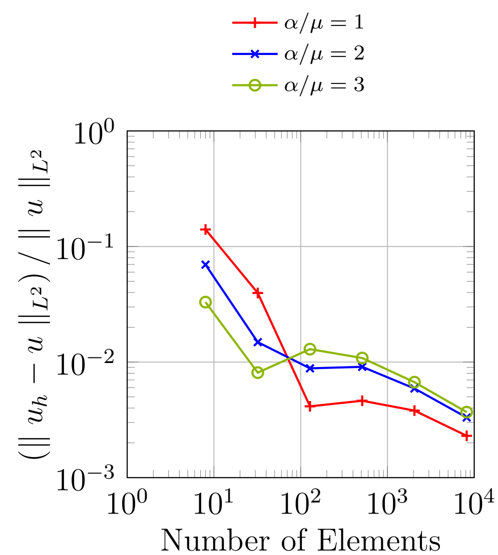

(a) Case two bubble function

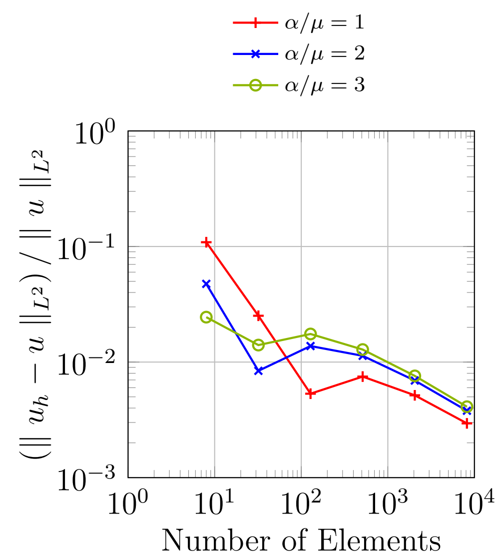

(b) Case two bubble function of which one mixed

Figure 16: Beam Cantilever: the relative error vs. the number of elements measured relative to the L^2 norm (regular mesh)

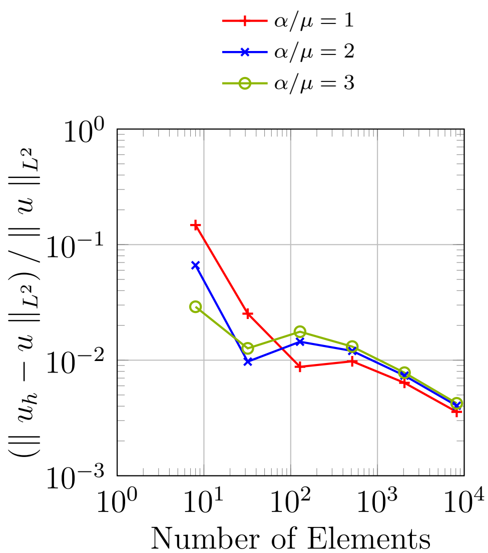

(a) Type 1

(b) Type 2

Figure 17: Beam Cantilever: the relative error vs. the number of elements measured relative to the L^2 norm (trapezoidal mesh)

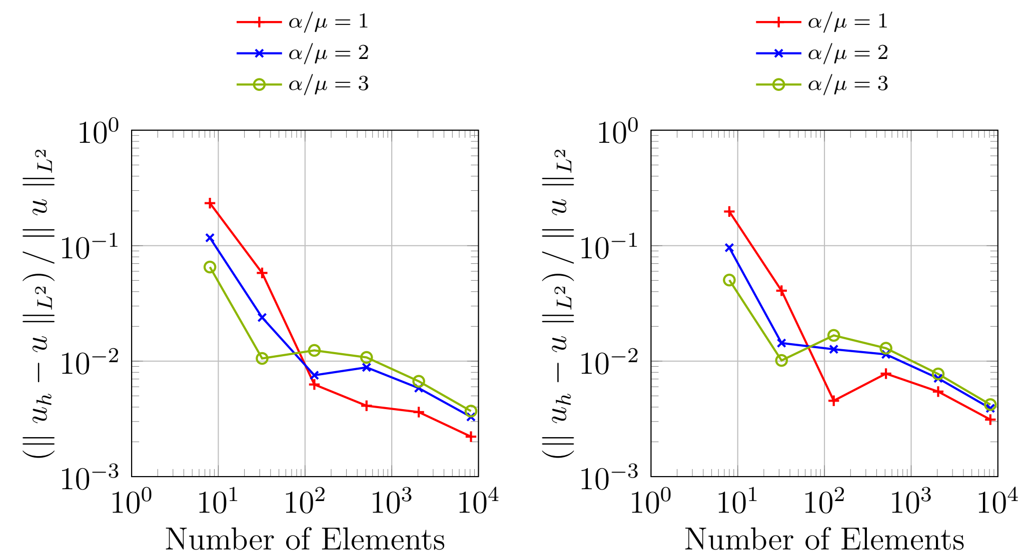

(a) Case two bubble function

(b) Case two bubble function of which one mixed

Figure 18: Beam Cantilever: the relative error vs. the number of elements measured relative to the L^2 norm (trapezoidal mesh)

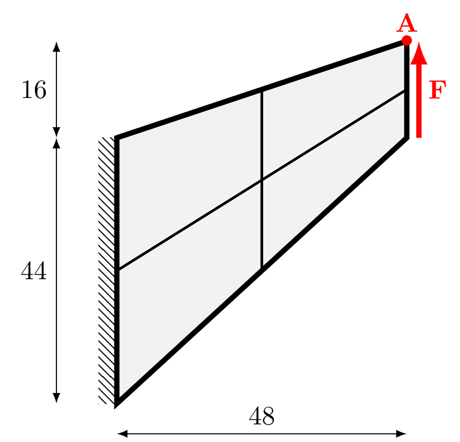

Figure 19: Cook's Membrane geometry

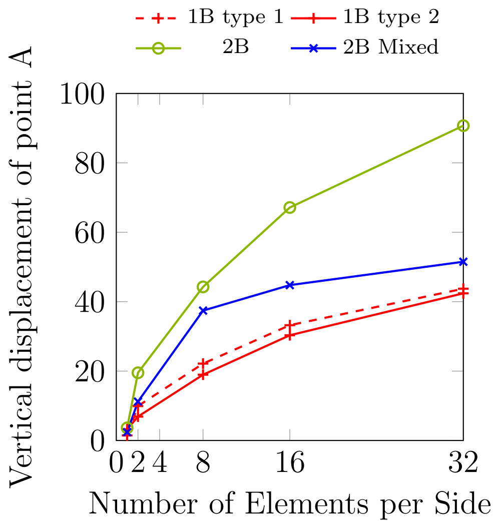

(a) $\alpha = 1$

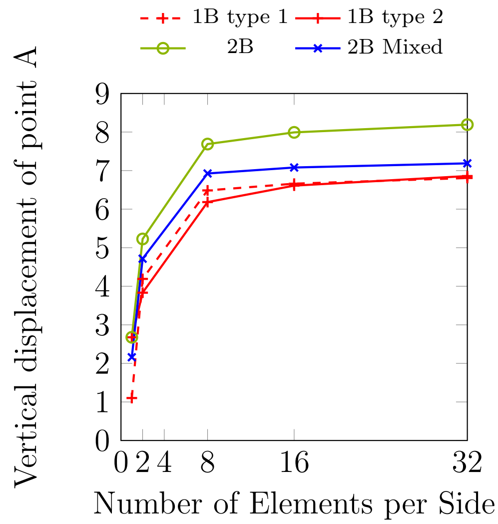

(b) $\alpha/\mu = 1$

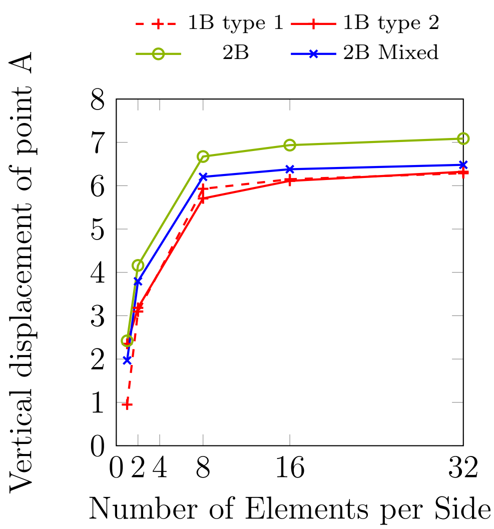

(c) $\alpha/\mu = 2$

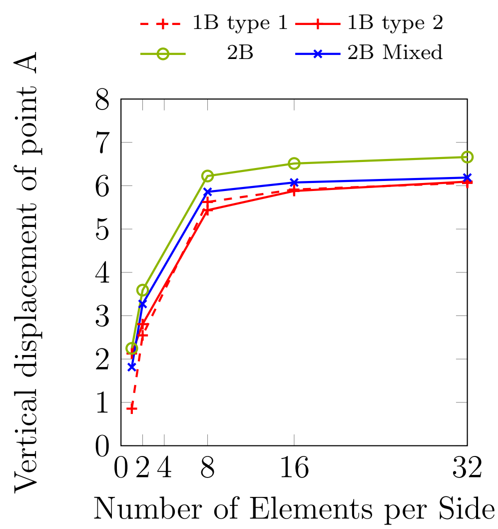

(d) $\alpha/\mu = 3$

Figure 20: Vertical Displacement of point A vs. the number of elements per side